ACS NANO

www.acsnano.org

ARTICLE

Atomic Layer Deposition of Stable $LiAlF_4$ Lithium Ion Conductive Interfacial Layer for Stable Cathode Cycling

Jin Xie,[†] Austin D. Sendek,[‡] Ekin D. Cubuk,[†] Xiaokun Zhang,[†] Zhiyi Lu,[†] Yongji Gong,[†] Tong Wu,[†] Feifei Shi,[†] Wei Liu,[†] Evan J. Reed,[†] and Yi Cui*[,†,§]

[†]Department of Materials Science and Engineering and [‡]Department of Applied Physics, Stanford University, Stanford, California 94305, United States

[§]Stanford Institute for Materials and Energy Sciences, SLAC National Accelerator Laboratory, 2575 Sand Hill Road, Menlo Park, California 94025, United States

Supporting Information

ABSTRACT: **Modern lithium ion batteries are often desired to operate at a wide electrochemical window to maximize energy densities. While pushing the limit of cutoff potentials allows batteries to provide greater energy densities with enhanced specific capacities and higher voltage outputs, it raises key challenges with thermodynamic and kinetic stability in the battery. This is especially true for layered lithium transition-metal oxides, where capacities can improve but stabilities are compromised as wider electrochemical windows are applied. To overcome the above-mentioned challenges, we used atomic layer deposition to develop a $LiAlF_4$ solid thin film with robust stability and satisfactory ion conductivity, which is superior to commonly used LiF and AlF_3. With a predicted stable electrochemical window of approximately 2.0 ± 0.9 to 5.7 ± 0.7 V *vs* Li^+/Li for $LiAlF_4$, excellent stability was achieved for high Ni content $LiNi_{0.8}Mn_{0.1}Co_{0.1}O_2$ electrodes with $LiAlF_4$ interfacial layer at a wide electrochemical window of 2.75−4.50 V *vs* Li^+/Li.**

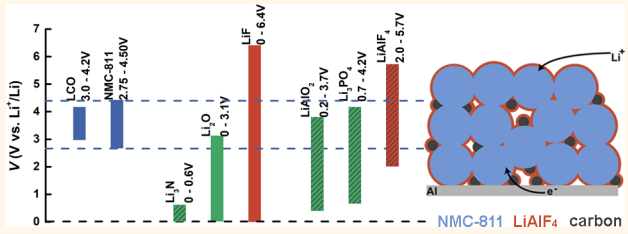

KEYWORDS: *lithium ion batteries, layered lithium transition-metal oxide, atomic layer deposition, lithium aluminum fluoride, lithium ion conductive interfacial layer, surface coating*

Driven by increasing energy storage demands in consumer electronics, electrical vehicles, and even grid scale power, modern lithium ion batteries are often desired to operate at wide electrochemical windows for enhanced specific capacities and higher voltage outputs.[1,2] Operating at extreme voltages posts grand challenges in the field of materials research, as issues with instability plague the electrodes, electrolytes, and their interfaces. To maintain a long cycle life, developing a stable interfacial layer is critical, as degradation typically starts to propagate where the electrode and electrolyte meet.[3,4] The accumulation of byproducts at the interface leads to high internal resistance, which can eventually cause battery failure. In the past few decades, great efforts have been devoted to achieve a stable interfacial layer. A great example of such is the solid−electrolyte interphase (SEI) formation on the graphite anode, which enabled the commercialization of lithium ion batteries in the 1990s.[5] On the cathode side, the need to develop a stable interfacial layer is more and more important nowadays as its instability has become a limiting factor for batteries to operate safely for tens of years, especially when the cutoff potentials have been aggressively pushed to more positive for greater energy output.[2,6]

To solve the challenge, various methods including, but not limited to, surface coating,[7] surface modification by doping,[8,9] and electrolyte additive formulation[10] have been studied. To date, thin films including Al_2O_3,[11,12] AlF_3,[13,14] and lithium containing compounds (*e.g.*, $LiNi_{0.5}Mn_{0.5}O_2$,[15] $LiFePO_4$,[16] Li_2MnO_3,[17] and Li_2ZrO_3[18] for improved capacity and lithium ion conductivity) have been successfully deposited using different coating methods with varying levels of successes. However, a superior film which satisfies all major requirements simultaneously including electrochemically inert, chemically stable, lithium ion conductive, and highly uniform is still missing. In this study, we report a $LiAlF_4$ thin film prepared by atomic layer deposition (ALD) which satisfies all four requirements mentioned above for cathode to operate at wide electrochemical windows. We studied the effect of coating

Received: April 12, 2017
Accepted: June 30, 2017
Published: June 30, 2017

DOI: 10.1021/acsnano.7b02561
ACS Nano XXXX, XXX, XXX−XXX

on high Ni content $LiNi_{0.8}Mn_{0.1}Co_{0.1}O_2$ (NMC-811) cycled at 2.75−4.50 V *vs* Li^+/Li. The high Ni content layered lithium transition-metal oxides have attracted great interest, owing to their high capacity and low cost.[19,20] However, the replacement of Co with Ni reduces the structural stability, especially at high applied potentials and on the interface.[21] The film we developed served as a stable and lithium permeable interfacial layer for NMC-811. Good cycling stability can be obtained for 300 cycles with capacity retention higher than 99.9% per cycle at a wide electrochemical window of 2.75−4.50 V *vs* Li^+/Li.

RESULTS/DISCUSSION

The interface between electrode and electrolyte is one of the most important components of the battery. It must be stable enough to withstand years of battery operation without degradation while retaining low resistance for lithium ions to diffuse through. Therefore, in order for the interfacial layer to work properly to enhance the stability of the cathode rather than to limit its performance, a few requirements need to be met simultaneously.

First, the interfacial layer has to be electrochemically and chemically stable to withstand the harsh battery operation conditions. To avoid the risk of decomposition by reduction or oxidation during cycling, the electrochemical stability window of the interfacial layer has to be wide enough so that it does not participate in the redox reactions. In Figure 1a, we provided the stability windows of a few candidate lithium containing compounds for this purpose, as reported by Richards *et al.*[22]

a

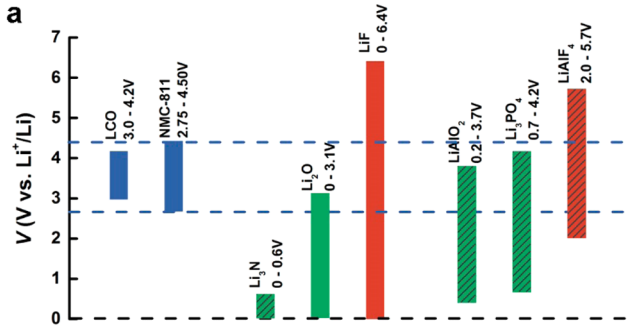

b

	Electrochemical stability	Chemical stability	Li ion conductivity
Li_3N	X	X	✓✓
Li_2O	X	X	X
LiF	✓✓	✓✓	X
$LiAlO_2$	X	✓	✓
Li_3PO_4	X	✓	✓
$LiAlF_4$	✓✓	✓✓	✓

Figure 1. (a) Calculated electrochemical stability windows of Li_3N, Li_2O, LiF, $LiAlO_2$, Li_3PO_4, and $LiAlF_4$. The windows of the first five candidates have been reported[22] (please see the Methods section and Supporting Information for detailed calculation of the decomposition potentials and reactions); we use DFT to calculate the window of $LiAlF_4$. The operating electrochemical window of NMC-811 in this study and typical operation electrochemical window of $LiCoO_2$ are included for comparison. (b) Selection criteria (chemical stability, electrochemical stability, and Li ion conductivity) of a few interfacial materials.

using the formation energy reported in the Materials Project database.[23] Among them, nitrides (*e.g.*, Li_3N, 0−0.6 V *vs* Li^+/Li), oxides (*e.g.*, Li_2O, 0−3.1 V *vs* Li^+/Li; $LiAlO_2$, 0.2−3.7 V *vs* Li^+/Li), and phosphate (*e.g.*, Li_3PO_4, 0.7−4.2 V *vs* Li^+/Li) are thermodynamically unstable (see Supporting Information for detailed calculation) in the range where lithiation/delithiation of layered lithium transition-metal oxides take place and therefore are prone to be decomposed by oxidation with years of battery operation. For comparison, fluorides are promising thanks to their superior stability. The stability window is as wide as 0−6.4 V *vs* Li^+/Li for LiF, a binary fluoride compound. Using these same methods, we find that the stability window of the fluorides remains wide even with the addition of second metal ions. We perform density functional theory (DFT) calculations on $LiAlF_4$ and find a formation energy of −3.547 eV/atom or −2053.4 kJ/mol for $LiAlF_4$ and predict an electrochemical window of 2.0 ± 0.9 to 5.7 ± 0.7 V *vs* Li^+/Li (see Methods section and Supporting Information for detailed calculation and error estimate). As seen in the far right bar in Figure 1a, our calculations indicate $LiAlF_4$ is thermodynamically stable in the entire operation window of the layered lithium transition-metal oxides, unlike most other candidates. Experimentally, cyclic voltammetry scans and XPS characterization were performed for $LiAlF_4$ films. The results also show that $LiAlF_4$ is stable in the electrochemical window of 2.75−4.50 V *vs* Li^+/Li (see Supporting Information for more details). In addition to its wide electrochemical window, fluoride compounds have superior chemical stability at the interface when compared with other chemical compositions. For example, oxides and nitrides would be attacked by trace amounts of H_2O and HF in the electrolyte. Even in the ambient air, fluorides are considered to be more resistant against moisture and CO_2 than oxides and nitrides, which makes the handling and processing of coated electrodes easier.

Second, the interfacial layers have to be lithium ion conductive to maintain the power density of the battery. A uniform coating of poor lithium ion conductors such as metal oxides (Al_2O_3[11,12] and AlF_3[13,24]) often induces an increased overpotential and a reduced capacity. In order to minimize the ion resistance, lithium containing thin films (Li_3N,[25] LiF,[26,27] $LiAlO_2$,[28] LiPON,[29] and $LiFePO_4$[16]) have been studied. Among them, fluorides are particularly promising due to the above-mentioned stability. While LiF is a poor lithium ion conductor, mixing LiF with divalent fluoride or trivalent fluoride has shown improved lithium ion conductivity.[30] Before this work, $LiAlF_4$ has not been used in lithium ion batteries experimentally, although $LiAlF_4$ has shown success in electrochromic devices using evaporation methods.[31−33]

Last but not the least, the interfacial layer needs to be uniform across the large high surface area of the electrode. While solution-phase coating methods on individual particles of cathode materials hold the advantages of being cost-effective and easy integration for large scale production, the non-uniformity is inherent upon postgrowth annealing, and film cracking may take place during slurry making and/or calendaring processes. Due to the complexity and compatibility of synthesis, there is no report of $LiAlF_4$ synthesis other than physical evaporation, to the best of our knowledge. However, evaporation methods limit the application of $LiAlF_4$ to devices with a planar geometry.[32,33] Compared to the above-mentioned methods, ALD could achieve uniform coating on high surface area electrodes directly.

DOI: 10.1021/acsnano.7b02561
ACS Nano XXXX, XXX, XXX−XXX

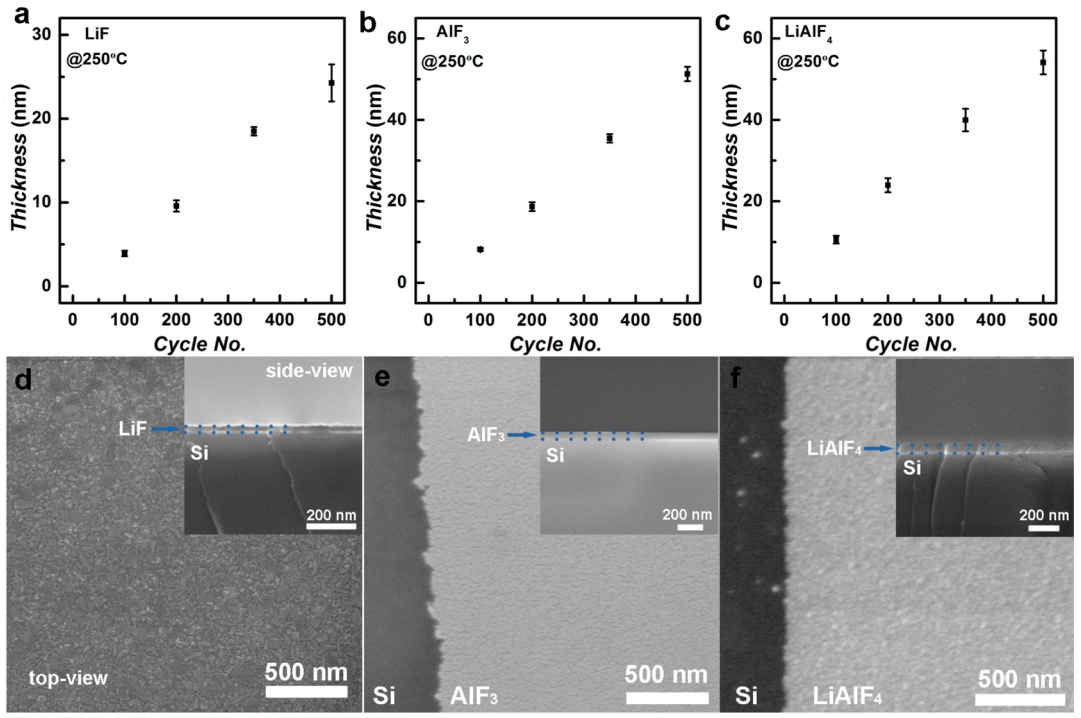

Figure 2. (a–c) Thickness characterization of LiF, AlF_3, and $LiAlF_4$ films with different ALD cycle numbers. (d–f) Top-view SEM images of ALD LiF, AlF_3, and $LiAlF_4$ films on silicon wafers. Inset images are side-view images (view angle of 90°) of ALD LiF, AlF_3, and $LiAlF_4$ films on silicon wafers.

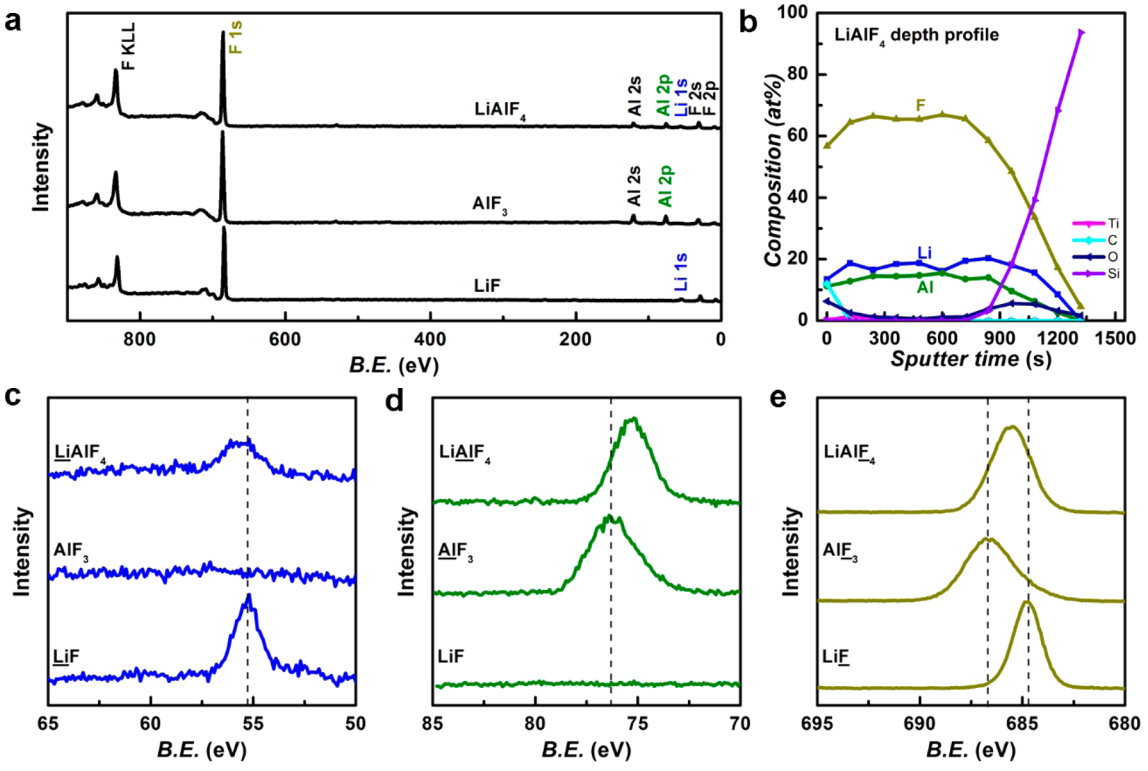

Figure 3. XPS characterizations. (a) XPS characterizations of ALD grown LiF, AlF_3, and $LiAlF_4$ films. (b) Depth profile of $LiAlF_4$ film prepared by ALD. (c–e) Fine XPS scans of Li 1s peaks, Al 2p peaks, and F 1s peaks of LiF, AlF_3, and $LiAlF_4$ films.

ALD LiF deposition was first reported by Mantymaki *et al.* using lithium bis(2,2,6,6-tetramethyl-3,5-heptanedionate) (Lithd) and TiF_4 as precursors.[26] The deposition is challenging as the growth is temperature gradient dependent, requires a large Lithd dose, and has a poor adhesion to the substrate. Although these drawbacks can be partially overcome by introducing $Mg(thd)_2$ subcycles,[27] the process is unnecessarily complicated. In this study, we propose a different LiF ALD

DOI: 10.1021/acsnano.7b02561
ACS Nano XXXX, XXX, XXX–XXX

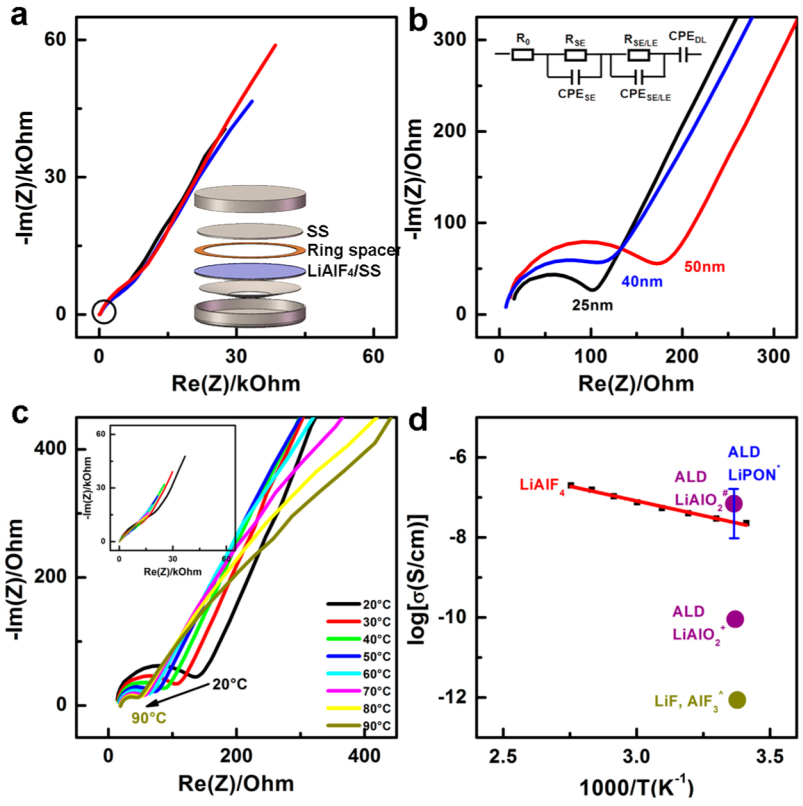

Figure 4. (a) EIS characterizations of $LiAlF_4$ films with different thicknesses at room temperature, inset shows the EIS characterization setup. (b) Enlarged EIS spectra shown in (a), inset shows the equivalent circuit. (c) EIS characterizations at different temperatures. (d) Conductivity *vs* temperature plot of $LiAlF_4$ film and reported lithium ion conductivities of evaporated LiF and AlF_3 films,[30] ALD deposited $LiAlO_2$,[39,40] and ALD deposited LiPON[29] films.

chemistry based on lithium *tert*-butoxide as the lithium source. Lithium *tert*-butoxide has a relatively high vapor pressure[34] and good thermal stability among different lithium organometallic compounds.[35] LiF thin films can be acquired at growth temperatures ranging from 200 to 300 °C (see Supporting Information for more detailed characterizations). The highest growth rate achieved was 0.5 Å per ALD cycle at 250 °C. At 250 °C, the coverage of LiF deposition is uniform and featured small grains (Figure 2d). The AlF_3 deposition was done following literature reports.[36] The deposition rate of AlF_3 at 250 °C is close to 1 Å per ALD cycle. Unlike LiF which shows individual grains, an AlF_3 film prepared by ALD is uniform and featureless (Figure 2e). ALD provides great flexibility to prepare complex films by integrating different recipes. In this study, $LiAlF_4$ film was prepared by introducing alternative subcycles of LiF (LiOtBu and TiF_4) and AlF_3 ($AlCl_3$ and TiF_4). The $LiAlF_4$ prepared by this method is uniform (Figure 2f) as well and its thicknesses increased linearly with total ALD cycles (Figure 2c). Among three ALD films, LiF thin film prepared by ALD is crystalline, while AlF_3 and $LiAlF_4$ thin films prepared by ALD are amorphous (see Supporting Information for grazing incidence X-ray diffraction (GIXRD) characterization).

XPS characterizations were carried out to analyze chemical compositions of ALD grown films (Figure 3). The ALD LiF film showed a distinct Li 1s peak and F 1s peak at 55.3 and 684.8 eV, both agreeing well with literature reports for bulk LiF.[37] The ALD AlF_3 film showed a clear Al 2p peak at 76.2 eV, also in agreement with reported values for bulk AlF_3.[37] Due to the higher electronegativity of Al compared to Li, the F 1s peak in AlF_3 shifted to higher binding energy compared to the F 1s peak in LiF. The observed peak position of 686.5 eV was close to the F 1s peak in α-AlF_3.[38] ALD $LiAlF_4$ film had all three elements with Li 1s, Al 2p, and F 1s peaks sitting at 55.6, 75.3, and 685.5 eV. Compared to ALD LiF and AlF_3 films, the Li 1s peak in the $LiAlF_4$ film shifted to higher binding energy, and the Al 2p peak in the $LiAlF_4$ film shifted to lower binding energy as expected. The F 1s peak in $LiAlF_4$ film also shifted to higher binding energy compared to the F 1s peak in LiF, but lower binding energy compared to the F 1s peak in AlF_3. The peak position analysis demonstrated that the $LiAlF_4$ film forms one single chemical composition rather than a physical mixture of LiF and AlF_3.

The depth profile of $LiAlF_4$ film was also investigated (Figure 3b). The C and O impurities on the surface were low and quickly disappeared after the first sputtering cycle, indicating the nature of surface absorbed impurities. Ti, C, and O impurities remained low throughout the entire film. The Li:Al:F atomic ratio was consistent across different film depths with an average being 1.2:1.0:4.5 according to XPS. For comparison, the F/Li atomic ratio in ALD LiF film and F/Al atomic ratio in ALD AlF_3 film were 0.97 and 3.45, respectively (see Supporting Information). Previous reports of AlF_3 ALD also show an excess of fluorine compared to metal ions using a different cauterization method (time-of-flight elastic recoil detection analysis).[36] The excess of fluorine may create metal vacancies in ALD grown films for enhanced lithium ion conductivity.

The lithium ion conductivity of ALD $LiAlF_4$ film was tested by depositing films with different thicknesses onto stainless steel substrates, which were then assembled into coin cells (the

DOI: 10.1021/acsnano.7b02561
ACS Nano XXXX, XXX, XXX−XXX

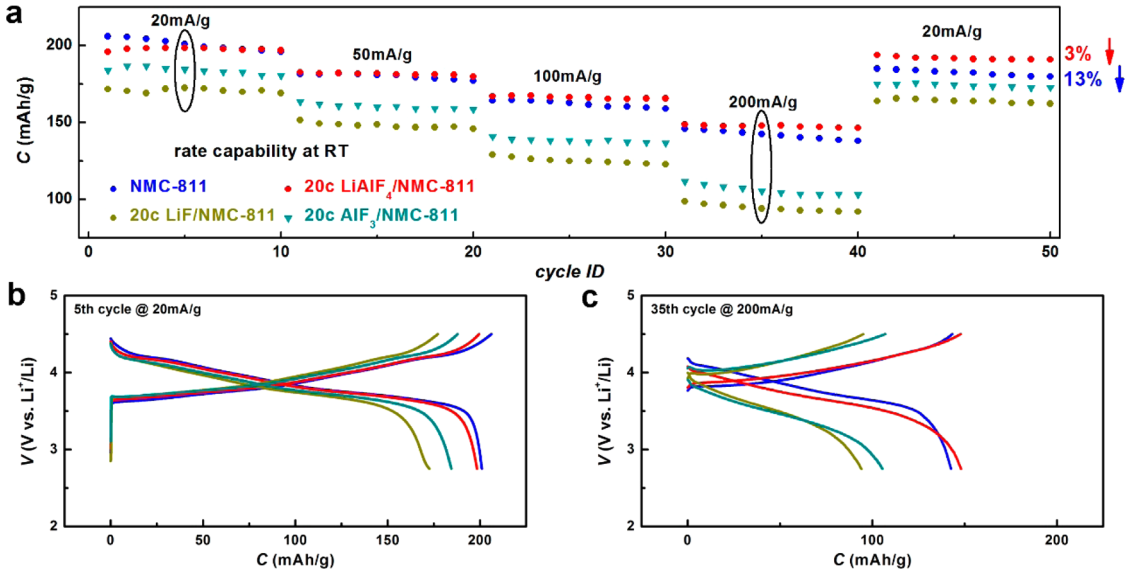

Figure 5. (a) Rate performance of pristine, 20c ALD $LiAlF_4$ coated, 20c ALD LiF coated, and 20c ALD AlF_3 coated NMC-811 electrodes at room temperature with an electrochemical window of 2.75−4.50 V *vs* Li^+/Li. (b, c) Voltage *vs* capacity plots of pristine, 20c ALD $LiAlF_4$ coated, 20c ALD LiF coated, and 20c ALD AlF_3 coated NMC-811 electrodes at 5th and 35th cycles, respectively.

setup is shown as the inset of Figure 4a). Figure 4a,b shows the electrochemical impedance spectroscopic (EIS) spectra of $LiAlF_4$ films as a function of film thickness. The conductivity was determined to be $3.5 \pm 0.5 \times 10^{-8}$ S/cm using an equivalent circuit model, shown as an inset of Figure 4b. The measurement of lithium ion conductivity in the liquid cell setup has been reported previously.[29,41] The equivalent circuit consists of two parallel R/CPE at both high (CPE_{SE}/R_{SE}) and medium ($CPE_{SE/LE}/R_{SE/LE}$) frequencies. CPE_{SE}/R_{SE} describes ionic conduction processes in the $LiAlF_4$ film and $CPE_{SE/LE}/R_{SE/LE}$ describes ionic conduction processes across the solid−electrolyte interface. Additionally, R_0 is used to describe the electrolyte and contact resistance, and CPE_{DL} is used to describe the capacitance at the electrode interface. The measured lithium ion conductivity of ALD $LiAlF_4$ is 4 orders of magnitude higher than that of LiF or AlF_3 reported in the literature.[30] For comparison purposes, the lithium ion conductivities of other lithium containing films (LiPON[29] and $LiAlO_2$[39,40]) prepared by ALD are also plotted in Figure 4d. The conductivity of $LiAlF_4$ reported here is close to ALD grown LiPON. However, the advantage of using $LiAlF_4$ is its wide electrochemical stability window, which allows it to be used as a protection film on cathode materials without being oxidized or reduced.

High Ni content layered lithium transition-metal oxides are attractive and promising due to low cost and high capacity. Although NMC-811 (~80% Ni content, see Supporting Information for basic materials characterization of NMC-811 tested in this study) could deliver a capacity exceeding 200 mAh/g at a wide electrochemical window (2.75−4.50 V *vs* Li^+/Li), it is often limited to cycle at a much narrower electrochemical window to maintain proper long-term stability (see Supporting Information for its cycle stabilities at different electrochemical windows). Previous work by Li *et al.*[21] has shown that the fast capacity decay is related to the interface instability when cycled at a wide electrochemical window. In this study, we show the long-term stability has been improved significantly, and rate performance has not been compromised when the $LiAlF_4$ interfacial layer was applied using ALD.

The ALD $LiAlF_4$ thin film coating was performed directly on the NMC-811 electrodes instead of NMC-811 particles. The surface coating mechanism of the ALD technique ensures the coating occurs on the surface, generating an uniform thin film covering the entire electrode while maintaining the interconnectivity of the NMC-811 particles (see Supporting Information for SEM characterization of NMC-811 electrodes before and after ALD $LiAlF_4$ coating). In Figure 5, we tested the rate performance of pristine and ALD coated NMC-811 electrodes with an electrochemical window of 2.75−4.50 V *vs* Li^+/Li. At the lowest rate of 20 mA/g, the discharge capacity of pristine NMC-811 electrode quickly dropped from 206.0 mAh/g to 195.9 mAh/g within the first 10 cycles. While cathodes with 20 cycles of ALD LiF coating, AlF_3 coating, and $LiAlF_4$ coating all showed improved stability, their specific capacities were different. With the highest lithium ion conductivity among the three, $LiAlF_4$ coated electrode delivered an average capacity of 197.7 mAh/g at 20 mA/g during 1−10th cycles and 147.6 mAh/g at 200 mA/g during 31−41st cycles, both of which were close to or even higher than pristine NMC-811 (200.8 mAh/g at 20 mA/g and 142.0 mAh/g at 200 mA/g). However, owing to the poor conductivity of LiF, a dense and uniform LiF coating on the surface of cathode materials would hinder the lithium ion transport and cause polarization. The average capacities of LiF coated electrodes were only 170.8 mAh/g at 20 mA/g during 1−10th cycles and 94.5 mAh/g at 200 mA/g during 31−41st cycles. While AlF_3 has been reported as a coating layer to stabilize both anodes[14] and cathodes[13,24,42] in lithium ion batteries, the mechanism of how lithium ion conducts through the coating layer is not clear. For instance, AlF_3 would convert to Li_3AlF_6, LiF, Al, and various Li_xAl_y alloys on the anode depending on how low an equilibrium potential is applied (see Supporting Information for detailed calculation). In addition to the lithium ion conductivity provided by some of these products, the phase transformation itself may leads to a porous film, which allows lithium ions to pass through as well. However, the porosity of the film may leads to battery degradation by allowing interfacial reactions between electrode and electrolyte. On the cathode part, owing to the high

DOI: 10.1021/acsnano.7b02561
ACS Nano XXXX, XXX, XXX−XXX

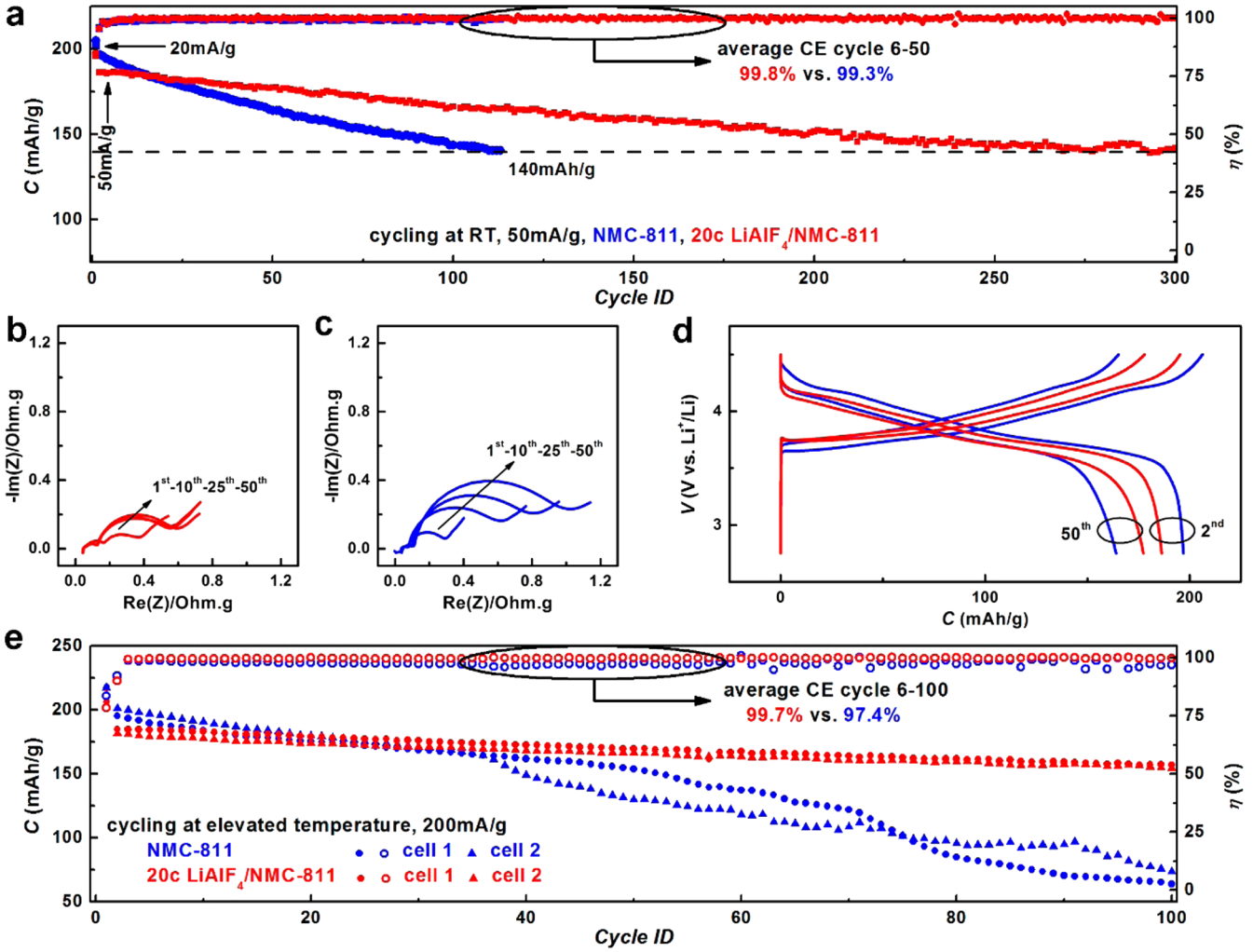

Figure 6. (a) Cycle performance of pristine and 20c ALD $LiAlF_4$ coated NMC-811 electrodes at room temperature with an electrochemical window of 2.75−4.50 V *vs* Li^+/Li. (b, c) EIS characterizations of pristine and 20c ALD $LiAlF_4$ coated NMC-811 electrodes after 1st, 10th, 25th, and 50th cycles. (d) Voltage *vs* capacity plots of pristine and 20c ALD $LiAlF_4$ coated NMC-811 electrodes at 2nd and 50th cycles. (e) Cycle performance of pristine and 20c ALD $LiAlF_4$ coated NMC-811 electrodes at elevated temperature (50 °C) with an electrochemical window of 2.75−4.50 V *vs* Li^+/Li.

operation voltage, it is unlikely for lithiation to take place in AlF_3 thermodynamically according to our thermodynamic calculation. As a result, a thicker coating has led to higher overpotential and reduced capacity in the past.[24] This phenomenon becomes more substantial when metal fluoride is applied using ALD, which is known for its conformity of coverage. The average capacities of AlF_3 coated electrodes were only 183.7 mAh/g at 20 mA/g and 106.0 mAh/g at 200 mA/g. A similar phenomenon has also been observed for other fluoride coating with only five ALD cycles.[43] The uniform ALD coating provides enhanced stability, but comes at the cost of serving as an additional lithium ion diffusion barrier. When the lithium ion conductivity of the film is low (such as LiF and AlF_3), such barriers lead to a high overpotential during cycling (Figure 5b,c) and thus a poor rate performance. Our results show that having a stable and lithium ion conductive interfacial layer is important.

The long-term stability of pristine and ALD $LiAlF_4$ coated NMC-811 electrodes was further analyzed using galvanostatic cycling at both room temperature and an elevated temperature (Figure 6) at a wide electrochemical window of 2.75−4.50 V *vs* Li^+/Li. At room temperature, the electrode with $LiAlF_4$ coating maintained a capacity higher than 140 mAh/g after 300 cycles (24% decay over 300 cycles or 0.08% per cycle). For pristine NMC-811, the capacity dropped quickly to <140 mAh/g after 113 cycles (29% decay over 113 cycles or 0.26% per cycle). The poor cycle stability at elevated temperatures is the most considerable drawback for high Ni content layered lithium metal oxides.[19,20,44] Therefore, testing the long-term cycle stability at elevated temperatures presents a rigorous, meaningful, and real-world relevant test for NMC-811. Thanks to the enhanced lithium ion conductivity of both the coating layer and NMC-811 itself at 50 °C, batteries were cycled at a higher rate of 200 mAh/g (Figure 6e). The capacities of both pristine NMC-811 electrodes decayed fast to <100 mAh/g within 100 cycles. In contrast, both ALD $LiAlF_4$ coated samples showed excellent capacity retention within 100 cycles.

Side reactions between electrode, in particular high oxidation state Ni^{4+}, and organic electrolyte have been reported to be one of the key failure mechanisms for high Ni content layered metal oxide.[45,46] The highly reactive Ni^{4+} ions can accelerate electrolyte decomposition, especially at high-applied potentials. The accumulation of side products would hinder lithium ion transport at the electrode−electrolyte interface. Therefore, it is

DOI: 10.1021/acsnano.7b02561
ACS Nano XXXX, XXX, XXX−XXX

important to develop an uniformly, chemically inert, electrochemically stable, and lithium ion conductive interface to achieve long-term stability for high Ni content layered lithium metal oxides. Such a stable and uniform interface in principle could minimize the parasitic reactions between the electrode (such as Ni^{4+}) and the electrolyte. In order to prove this hypothesis, the magnitude of parasitic reactions was monitored by measuring the Coulombic efficiency (CE) of the battery. The CE is defined as CE = capacity of discharge/capacity of charge. The cycle life of lithium ion battery is not infinite because small amounts of active materials (electrode and/or electrolyte) are consumed by parasitic reactions during each cycle. As Li is excess in the counter electrode in the NMC-811/Li half-cells, the detected CE lower than unity (100.0%) can be explained by the parasitic reactions on the cathode. When tested at room temperature, the average CE of pristine NMC-811 was 99.3%, indicating a high degree of parasitic reactions, such as electrolyte oxidation by highly reactive Ni^{4+} at high-applied potentials, took place. In contrast, the average CE of $LiAlF_4$/NMC-811 was 99.8%. The average CE dropped from 99.3% at room temperature to 97.4% at elevated temperature for pristine NMC-811. The decrease of CE suggests the magnitude of parasitic reactions increased at elevated temperature. With a stable and uniform ALD $LiAlF_4$ coating, the average CE improved significantly from 97.4% to 99.7% at elevated temperature. The difference we observed in our CE measurement strongly supports our hypothesis that the improvement of cycle stability by $LiAlF_4$ coating is through reduced parasitic reactions.

The parasitic reactions at the interface of electrode and electrolyte also cause the accumulation of side products on the surface of the cathode, and its accumulation can be detected using impedance spectroscopy.[45] As shown in Figure 6b,c, the impedance spectra of the battery at different cycle numbers were recorded. The impedance spectra of NMC-811 electrodes with and without $LiAlF_4$ coating comprised two semicircles and a straight line angled close to 45°. The small semicircle at high frequency was attributed to the solid−electrolyte interface (R_{SEI} and CPE_{SEI}), while the one at medium frequency corresponded to the charge transfer process at the cathode−electrolyte interface (R_{ct} and CPE_{ct}).[45] The 45° inclined line at low frequency was due to the Warburg impedance (Z_w), which was related to the diffusion of lithium ions within the cathode. Upon cycling, the semicircle at medium frequency increased significantly for the pristine NMC-811, indicating the slow-down of charge transport across the cathode−electrolyte interface. The charge transfer resistance at the electrode−electrolyte interface for both pristine NMC-811 and ALD $LiAlF_4$ coated NMC-811 after different numbers of cycles can be calculated (see Supporting Information for more details). Although the initial charge-transfer resistance was similar for both pristine NMC-811 and ALD $LiAlF_4$ coated NMC-811 after the first cycle, it increased much faster for pristine NMC-811 compared to ALD $LiAlF_4$ coated NMC-811 upon cycling. We also noticed that the voltage hysteresis increased slower for coated sample when compared to pristine NMC-811 (Figure 6d). The fact that the $LiAlF_4$ coating layer suppressed the fast impedance growth supports that $LiAlF_4$ film could minimize the magnitude of parasitic reactions at the electrode−electrolyte interface. While there may be other factors that could also contribute to the improved stability when $LiAlF_4$ is applied, the reduced parasitic reaction at the electrode−electrolyte interface is an important one as suggested by our CE analysis and impedance spectra analysis (see Supporting Information for a brief discussion of failure mechanisms and additional characterizations).

CONCLUSIONS

To summarize, we designed and synthesized a stable and lithium ion conductive $LiAlF_4$ interfacial layer on lithium ion battery cathodes using atomic layer deposition. Our calculations show that the fluoride-based interfacial layer is thermodynamically stable within a wide electrochemical window. The stable and lithium ion conductive interfacial layer improved the stability of high Ni content NMC-811 electrodes without sacrificing rate performance. If a stable interface between electrode and electrolyte can be achieved by rational materials design, lithium ion batteries with higher energy density and longer cycle life may find more applications including portable electronic, vehicle electrification, and grid-scale energy storage and beyond.

METHODS

DFT Calculations. To calculate the electrochemical window, we first calculated the formation energy of a crystalline form of $LiAlF_4$ and then used the phase diagram building tool in the Materials Project (MP) database.[47,48] To generate the $LiAlF_4$ structure, we substituted in F for Cl in the stable $LiAlCl_4$ structure in the MP database (MPID mp-22983) and fully relaxed the lattice vectors and the positions of the ions. The resulting formation energy is −3.55 eV/atom. This value is calculated at 0 K and 0 atm and uses a reference energy of zero for the pure elements. According to the MP phase diagram for the Li−Al−F ternary system, $LiAlF_4$ is predicted to oxidize at a potential of 5.72 V *vs* Li/Li^+ according to the following reaction:

$$LiAlF_4 \rightarrow Li + 0.5F_2 + AlF_3$$

The reducing reaction is predicted to occur at a potential of 2.05 V *vs* Li/Li^+ according to the following reaction:

$$LiAlF_4 + Li \rightarrow 2/3Li_3AlF_6 + 1/3Al$$

For the DFT calculations we use the Vienna *ab initio* Simulation Package (VASP)[49] with the generalized gradient approximation (GGA) of Perdew−Burke−Ernzerhof (PBE)[50] and the projector augmented wave (PAW)[51] method. We use the following pseudopotentials: PAW_PBE Li_sv, PAW_PBE Cl, and PAW_PBE F. We employ a plane wave cutoff energy of 520 eV and *k*-mesh with a density of at least 1500/atom.

We confirm experimentally the $LiAlF_4$ thin film is amorphous (see Supporting Information for GIXRD characterization), but perform the DFT formation energy calculation on a representative crystalline phase for computational tractability. Work on Si,[52,53] Ge,[54] and SiO_2[55] has been reported to indicate small and consistent energy differences between the crystalline and amorphous phases (~0.1 eV for Si) over compositional space during lithiation (*i.e.*, Li_xSi, Li_xGe, and Li_xSiO_2, respectively), suggesting that the electrochemical window of the crystalline phase may not be an unreasonable approximation of the amorphous phase. To estimate the uncertainty in this approximation, we introduce an error of ±0.1 eV/atom to all crystalline phases considered here. Propagating this error yields an uncertainty in the oxidation potential of ±0.7 V and an uncertainty in the reduction potential of ±0.9 V.

Materials Synthesis and Preparation. LiF deposition was performed using a Savannah S100 ALD system (Ultratech/Cambridge Nanotech). The LiF deposition consists of alternating pulse and purge of lithium *tert*-butoxide (99%, Alfa Aesar) and TiF_4 (Sigma-Aldrich) as precursors. TiF_4 was gently grinded prior to use. A typical pulse and purge durations for lithium *tert*-butoxide subcycle are 1 s and 15 s, respectively. A typical pulse and purge durations for TiF_4 subcycle are 0.1 s and 15 s, respectively. Lithium *tert*-butoxide was heated to 160−170 °C, and TiF_4 was kept at 120−130 °C. LiF thin films can be

DOI: 10.1021/acsnano.7b02561
ACS Nano XXXX, XXX, XXX−XXX

obtained at deposition temperatures ranging from 200 to 300 °C. AlF_3 ALD deposition was performed following literature reported recipes.[36] The AlF_3 deposition consists of alternating pulse and purge of $AlCl_3$ (>99%, Sigma-Aldrich) and TiF_4 as precursors. Typical pulse and purge durations for $AlCl_3$ subcycle are 0.1 s and 15 s, respectively. Typical pulse and purge durations for TiF_4 subcycle are 0.1 s and 15 s, respectively. Both $AlCl_3$ and TiF_4 precursors were kept at 120−130 °C. AlF_3 thin film was obtained at a deposition temperature of 250 °C. $LiAlF_4$ ALD deposition was performed by alternating LiF and AlF_3 subcycles with a 1:1 ratio. $LiAlF_4$ thin film was obtained at 250 °C. High-purity argon gas was used as the carrier gas and purging gas for all the ALD processes mentioned above.

Materials Characterizations. SEM images were captured in a FEI XL30 Sirion SEM. XPS was performed on PHI 5000 VersaProbe, using an Al Kα (λ = 0.83 nm, hυ = 1486.7 eV) X-ray source operated at 2 kV and 20 mA. A Woollam M2000 spectroscopic ellipsometer was used for measuring and fitting optical properties of ALD thin films on silicon substrates with native oxides.

Electrochemical Measurements. Electrochemical impedance spectroscopic (EIS) measurements were conducted using a Biologic VSP potentiostat over the frequency range from 0.1 Hz to 1 MHz in a temperature-controlled environmental chamber (BTU-133, ESPEC North American, Inc.) from 20 to 90 °C and then 80 to 0 °C. $LiAlF_4$ thin film was deposited on a stainless steel (SS) spacer. A coin cell was then assembled with a piece of $LiAlF_4$/SS spacer as the working electrode and a piece of bare SS spacer as the counter electrode. Liquid electrolyte with 1 M LiPF6 in 1:1 ethylene carbonate (EC) and diethyl carbonate (DEC) (BASF) was confined in between the two electrodes with a polyimide ring spacer.

NMC-811 powders were acquired from an industry partner (Li-Fun Tech.). Battery cycling performance was evaluated by the galvanostatic cycling of coin cells with NMC-811 or coated NMC-811 as working electrodes and Li foils as counter electrodes. The working electrodes were made through typical slurry-making, drying, and calendaring processes. LiF, AlF_3, and $LiAlF_4$ coatings were then applied on NMC-811 electrodes directly using ALD. For coin cell testing, 50 μL of 1 M LiPF6 in 1:1 EC and DEC (BASF) was added as the electrolyte. Battery cycling data were collected using a LAND 8-channel battery tester at both room temperature and 50 °C. EIS measurements for both pristine NMC-811 and coated NMC-811 were also conducted for coin cells after a certain number of cycles at room temperature.

ASSOCIATED CONTENT

Supporting Information

The Supporting Information is available free of charge on the ACS Publications website at DOI: 10.1021/acsnano.7b02561.

Experimental details and additional characterizations (PDF)

AUTHOR INFORMATION

Corresponding Author

*E-mail: yicui@stanford.edu.

ORCID

Jin Xie: 0000-0002-6270-1465

Feifei Shi: 0000-0002-9171-6180

Wei Liu: 0000-0002-6206-8321

Notes

The authors declare no competing financial interest.

ACKNOWLEDGMENTS

Part of this work was performed at the Stanford Nano Shared Facilities (SNSF) and Stanford Nanofabrication Facility (SNF). Y.C. acknowledges the support from the Assistant Secretary for Energy Efficiency and Renewable Energy, Office of Vehicle Technologies of the US Department of Energy under the Battery Materials Research Program and Battery500 Consortium.

REFERENCES

(1) Goodenough, J. B.; Kim, Y. Challenges for Rechargeable Li Batteries. *Chem. Mater.* **2010**, *22*, 587−603.

(2) Whittingham, M. S. Lithium Batteries and Cathode Materials. *Chem. Rev.* **2004**, *104*, 4271−4301.

(3) Palacín, M. R.; de Guibert, A. Why Do Batteries Fail? *Science* **2016**, *351*, 1253292.

(4) Xu, K.; von Cresce, A. Interfacing Electrolytes with Electrodes in Li Ion Batteries. *J. Mater. Chem.* **2011**, *21*, 9849−9864.

(5) Aurbach, D.; Markovsky, B.; Weissman, I.; Levi, E.; Ein-Eli, Y. On the Correlation Between Surface Chemistry and Performance of Graphite Negative Electrodes for Li Ion Batteries. *Electrochim. Acta* **1999**, *45*, 67−86.

(6) Ellis, B. L.; Lee, K. T.; Nazar, L. F. Positive Electrode Materials for Li-Ion and Li-Batteries. *Chem. Mater.* **2010**, *22*, 691−714.

(7) Li, C.; Zhang, H. P.; Fu, L. J.; Liu, H.; Wu, Y. P.; Rahm, E.; Holze, R.; Wu, H. Q. Cathode Materials Modified by Surface Coating for Lithium Ion Batteries. *Electrochim. Acta* **2006**, *51*, 3872−3883.

(8) Mladenov, M.; Stoyanova, R.; Zhecheva, E.; Vassilev, S. Effect of Mg Doping and MgO-Surface Modification on the Cycling Stability of $LiCoO_2$ Electrodes. *Electrochem. Commun.* **2001**, *3*, 410−416.

(9) Liu, H.; Zhang, Z.; Gong, Z.; Yang, Y. A Comparative Study of $LiNi_{0.8}Co_{0.2}O_2$ Cathode Materials Modified by Lattice-Doping and Surface-Coating. *Solid State Ionics* **2004**, *166*, 317−325.

(10) Choi, N.-S.; Han, J.-G.; Ha, S.-Y.; Park, I.; Back, C.-K. Recent Advances in the Electrolytes for Interfacial Stability of High-Voltage Cathodes in Lithium-Ion Batteries. *RSC Adv.* **2015**, *5*, 2732−2748.

(11) Cho, J.; Kim, Y. J.; Park, B. Novel $LiCoO_2$ Cathode Material with Al_2O_3 Coating for a Li Ion Cell. *Chem. Mater.* **2000**, *12*, 3788−3791.

(12) Jung, Y. S.; Cavanagh, A. S.; Dillon, A. C.; Groner, M. D.; George, S. M.; Lee, S. H. Enhanced Stability of $LiCoO_2$ Cathodes in Lithium-Ion Batteries Using Surface Modification by Atomic Layer Deposition. *J. Electrochem. Soc.* **2010**, *157*, A75−A81.

(13) Sun, Y.-K.; Cho, S.-W.; Lee, S.-W.; Yoon, C. S.; Amine, K. AlF_3-Coating to Improve High Voltage Cycling Performance of Li-$[Ni_{1/3}Co_{1/3}Mn_{1/3}]O_2$ Cathode Materials for Lithium Secondary Batteries. *J. Electrochem. Soc.* **2007**, *154*, A168−A172.

(14) Ding, F.; Xu, W.; Choi, D.; Wang, W.; Li, X.; Engelhard, M. H.; Chen, X.; Yang, Z.; Zhang, J.-G. Enhanced Performance of Graphite Anode Materials by AlF_3 Coating for Lithium-Ion Batteries. *J. Mater. Chem.* **2012**, *22*, 12745−12751.

(15) Sun, Y.-K.; Myung, S.-T.; Kim, M.-H.; Prakash, J.; Amine, K. Synthesis and Characterization of Li-$[(Ni_{0.8}Co_{0.1}Mn_{0.1})_{0.8}(Ni_{0.5}Mn_{0.5})_{0.2}]O_2$ with the Microscale Core-Shell Structure as the Positive Electrode Material for Lithium Batteries. *J. Am. Chem. Soc.* **2005**, *127*, 13411−13418.

(16) Wang, H.; Zhang, W.-D.; Zhu, L.-Y.; Chen, M.-C. Effect of $LiFePO_4$ Coating on Electrochemical Performance of $LiCoO_2$ at High Temperature. *Solid State Ionics* **2007**, *178*, 131−136.

(17) Song, B.; Li, W.; Yan, P.; Oh, S.-M.; Wang, C.-M.; Manthiram, A. A Facile Cathode Design Combining Ni-Rich Layered Oxides with Li-Rich Layered Oxides for Lithium-Ion Batteries. *J. Power Sources* **2016**, *325*, 620−629.

(18) Song, B.; Li, W.; Oh, S.-M.; Manthiram, A. Long-Life Nickel-Rich Layered Oxide Cathodes with a Uniform Li_2ZrO_3 Surface Coating for Lithium-Ion Batteries. *ACS Appl. Mater. Interfaces* **2017**, *9*, 9718−9725.

(19) Manthiram, A.; Song, B.; Li, W. A Perspective on Nickel-Rich Layered Oxide Cathodes for Lithium-Ion Batteries. *Energy Storage Mater.* **2017**, *6*, 125−139.

(20) Xu, J.; Lin, F.; Doeff, M. M.; Tong, W. A Review of Ni-Based Layered Oxides for Rechargeable Li-Ion Batteries. *J. Mater. Chem. A* **2017**, *5*, 874−901.

DOI: 10.1021/acsnano.7b02561
ACS Nano XXXX, XXX, XXX−XXX

(21) Li, J.; Downie, L. E.; Ma, L.; Qiu, W.; Dahn, J. R. Study of the Failure Mechanisms of $LiNi_{0.8}Mn_{0.1}Co_{0.1}O_2$ Cathode Material for Lithium Ion Batteries. *J. Electrochem. Soc.* **2015**, *162*, A1401−A1408.
(22) Richards, W. D.; Miara, L. J.; Wang, Y.; Kim, J. C.; Ceder, G. Interface Stability In Solid-State Batteries. *Chem. Mater.* **2016**, *28*, 266−273.
(23) Jain, A.; Ong, S. P. Commentary: the Materials Project: a Materials Genome Approach to Accelerating Materials Innovation. *APL Mater.* **2013**, *1*, 011002.
(24) Sun, Y.-K.; Lee, M.-J.; Yoon, C. S.; Hassoun, J.; Amine, K.; Scrosati, B. The Role of AlF_3 Coatings in Improving Electrochemical Cycling of Li-Enriched Nickel-Manganese Oxide Electrodes for Li-Ion Batteries. *Adv. Mater.* **2012**, *24*, 1192−1196.
(25) Ostreng, E.; Vajeeston, P.; Nilsen, O.; Fjellvag, H. Atomic Layer Deposition of Lithium Nitride and Carbonate Using Lithium Silylamide. *RSC Adv.* **2012**, *2*, 6315−6322.
(26) Mantymaki, M.; Hamalainen, J.; Puukilainen, E.; Munnik, F.; Ritala, M.; Leskela, M. Atomic Layer Deposition of LiF Thin Films from Lithd and TiF_4 Precursors. *Chem. Vap. Deposition* **2013**, *19*, 111−116.
(27) Mantymaki, M.; Hamalainen, J.; Puukilainen, E.; Sajavaara, T.; Ritala, M.; Leskela, M. Atomic Layer Deposition of LiF Thin Films from Lithd, $Mg(thd)_2$, and TiF_4 Precursors. *Chem. Mater.* **2013**, *25*, 1656−1663.
(28) Cao, H.; Xia, B. J.; Zhang, Y.; Xu, N. X. $LiAlO_2$-Coated $LiCoO_2$ as Cathode Material for Lithium Ion Batteries. *Solid State Ionics* **2005**, *176*, 911−914.
(29) Kozen, A. C.; Pearse, A. J.; Lin, C.-F.; Noked, M.; Rubloff, G. W. Atomic Layer Deposition of the Solid Electrolyte LiPON. *Chem. Mater.* **2015**, *27*, 5324.
(30) Oi, T. Ionic-Conductivity of LiF Thin-Films Containing Divalent or Trivalent Metal Fluorides. *Mater. Res. Bull.* **1984**, *19*, 451−457.
(31) Chen, J.; Zhu, Z.; Zhou, Y.; Wang, R.; Yan, Y. All-Solid-State Electrochromic Device: $WO_3/LiAlF_4$:Li/VO_2. *Proc. SPIE* **1995**, *2531*, 161−165.
(32) Oi, T.; Miyauchi, K.; Uehara, K. Electrochromism of WO_3/$LiAlF_4$/LiIn Thin-Film Overlayers. *J. Appl. Phys.* **1982**, *53*, 1823−1823.
(33) Li, C.-P.; Tenent, R. C.; Dillon, A. C.; Morrish, R. M.; Wolden, C. A. Improved Durability of WO_3 Nanocomposite Films Using Atomic Layer and Vapor Deposited Coatings. *ECS Electrochem. Lett.* **2012**, *1*, H24−H27.
(34) Hämäläinen, J.; Holopainen, J.; Munnik, F.; Hatanpää, T.; Heikkilä, M.; Ritala, M.; Leskelä, M. Lithium Phosphate Thin Films Grown by Atomic Layer Deposition. *J. Electrochem. Soc.* **2012**, *159*, A259−A263.
(35) Putkonen, M.; Aaltonen, T.; Alnes, M.; Sajavaara, T.; Nilsen, O.; Fjellvag, H. Atomic Layer Deposition of Lithium Containing Thin Films. *J. Mater. Chem.* **2009**, *19*, 8767−8771.
(36) Mantymaki, M.; Heikkila, M. J.; Puukilainen, E.; Mizohata, K.; Marchand, B.; Raisanen, J.; Ritala, M.; Leskela, M. Atomic Layer Deposition of AlF_3 Thin Films Using Halide Precursors. *Chem. Mater.* **2015**, *27*, 604−611.
(37) Moulder, J. F.; Chastain, J. *Handbook of X-ray Photoelectron Spectroscopy: a Reference Book of Standard Spectra for Identification and Interpretation of XPS Data*. Physical Electronics, Inc.: Chanhassen, MN, 1995.
(38) Makarowicz, A.; Bailey, C. L.; Weiher, N.; Kemnitz, E.; Schroeder, S. L. M.; Mukhopadhyay, S.; Wander, A.; Searle, B. G.; Harrison, N. M. Electronic Structure of Lewis Acid Sites on High Surface Area Aluminium Fluorides: a Combined XPS and *ab initio* Investigation. *Phys. Chem. Chem. Phys.* **2009**, *11*, 5664−5673.
(39) Park, J. S.; Meng, X. B.; Elam, J. W.; Hao, S. Q.; Wolverton, C.; Kim, C.; Cabana, J. Ultrathin Lithium-Ion Conducting Coatings for Increased Interfacial Stability in High Voltage Lithium-Ion Batteries. *Chem. Mater.* **2014**, *26*, 3128−3134.
(40) Hu, Y.; Ruud, A.; Miikkulainen, V.; Norby, T.; Nilsen, O.; Fjellvag, H. Electrical Characterization of Amorphous $LiAlO_2$ Thin Films Deposited by Atomic Layer Deposition. *RSC Adv.* **2016**, *6*, 60479−60486.
(41) Busche, M. R.; Drossel, T.; Leichtweiss, T.; Weber, D. A.; Falk, M.; Schneider, M.; Reich, M.-L.; Sommer, H.; Adelhelm, P.; Janek, J. Dynamic Formation of a Solid-Liquid Electrolyte Interphase and Its Consequences for Hybrid-Battery Concepts. *Nat. Chem.* **2016**, *8*, 426−434.
(42) Zheng, J.; Gu, M.; Xiao, J.; Polzin, B. J.; Yan, P.; Chen, X.; Wang, C.; Zhang, J.-G. Functioning Mechanism of AlF_3 Coating on the Li- and Mn-Rich Cathode Materials. *Chem. Mater.* **2014**, *26*, 6320−6327.
(43) Park, J. S.; Mane, A. U.; Elam, J. W.; Croy, J. R. Amorphous Metal Fluoride Passivation Coatings Prepared by Atomic Layer Deposition on $LiCoO_2$ for Li-ion Batteries. *Chem. Mater.* **2015**, *27*, 1917−1920.
(44) Liu, W.; Oh, P.; Liu, X.; Lee, M.-J.; Cho, W.; Chae, S.; Kim, Y.; Cho, J. Nickel-Rich Layered Lithium Transition-Metal Oxide for High-Energy Lithium-Ion Batteries. *Angew. Chem., Int. Ed.* **2015**, *54*, 4440−4457.
(45) Chen, C. H.; Liu, J.; Amine, K. Symmetric Cell Approach and Impedance Spectroscopy of High Power Lithium-Ion Batteries. *J. Power Sources* **2001**, *96*, 321−328.
(46) Xia, J.; Ma, L.; Nelson, K. J.; Nie, M.; Lu, Z.; Dahn, J. R. A Study of Li-Ion Cells Operated to 4.5 V and at 55°C. *J. Electrochem. Soc.* **2016**, *163*, A2399−A2406.
(47) Ping Ong, S.; Wang, L.; Kang, B.; Ceder, G. Li-Fe-P-O_2 Phase Diagram from First Principles Calculations. *Chem. Mater.* **2008**, *20*, 1798−1807.
(48) Ong, S. P.; Jain, A.; Hautier, G.; Kang, B.; Ceder, G. Thermal Stabilities of Delithiated Olivine MPO_4 (M = Fe, Mn) Cathodes Investigated Using First Principles Calculations. *Electrochem. Commun.* **2010**, *12*, 427−430.
(49) Kresse, G.; Furthmüller, J. Efficient Iterative Schemes for *ab initio* Total-Energy Calculations Using a Plane-Wave Basis Set. *Phys. Rev. B: Condens. Matter Mater. Phys.* **1996**, *54*, 11169−11186.
(50) Perdew, J. P.; Burke, K.; Ernzerhof, M. Generalized Gradient Approximation Made Simple. *Phys. Rev. Lett.* **1996**, *77*, 3865−3868.
(51) Blöchl, P. E. Projector Augmented-Wave Method. *Phys. Rev. B: Condens. Matter Mater. Phys.* **1994**, *50*, 17953−17979.
(52) Kim, H.; Chou, C.-Y.; Ekerdt, J. G.; Hwang, G. S. Structure and Properties of Li-Si Alloys: a First-Principles Study. *J. Phys. Chem. C* **2011**, *115*, 2514−2521.
(53) Cubuk, E. D.; Kaxiras, E. Theory of Structural Transformation in Lithiated Amorphous Silicon. *Nano Lett.* **2014**, *14*, 4065−4070.
(54) Morris, A. J.; Grey, C. P.; Pickard, C. J. Thermodynamically Stable Lithium Silicides and Germanides from Density Functional Theory Calculations. *Phys. Rev. B: Condens. Matter Mater. Phys.* **2014**, *90*, 054111.
(55) Ostadhossein, A.; Kim, S.-Y.; Cubuk, E. D.; Qi, Y.; van Duin, A. C. T. Atomic Insight into the Lithium Storage and Diffusion Mechanism of SiO_2/Al_2O_3 Electrodes of Lithium Ion Batteries: ReaxFF Reactive Force Field Modeling. *J. Phys. Chem. A* **2016**, *120*, 2114−2127.

DOI: 10.1021/acsnano.7b02561
ACS Nano XXXX, XXX, XXX−XXX